



Effect of conjugate heat transfer on the thermo-electro-hydrodynamics of nanofluids: entropy optimization analysis

Rajkumar Sarma¹ · Abhay Kumar Shukla¹ · Harshad S. Gaikwad¹ · Pranab Kumar Mondal¹ · Somchai Wongwises²

Received: 28 May 2020 / Accepted: 5 October 2020 / Published online: 29 October 2020
© Akadémiai Kiadó, Budapest, Hungary 2020

Abstract

We investigate, in this analysis, the entropy generation characteristics associated with the transport of nanofluid in a microfluidic channel under the combined influences of applied pressure gradient and electrical forcing. In our study, the nanofluid is subjected to an asymmetric cooling at the channel walls, while the conductive transport of heat through the channel walls is also taken into account. We show that the underlying thermo-electro-hydrodynamics of nanofluids in the channel lead to entropy generation, attributed to the irreversibilities associated with heat transfer, viscous dissipation, and Joule heating effects. We establish that a non-trivial interplay among these irreversibilities gives rise to an optimum value of the geometrical parameter, viz. the channel wall thickness (δ), and the thermophysical parameters, viz. the thermal conductivity of the wall (γ), Biot number (Bi), and the modified Peclet number (\overline{Pe}), leading to a minimum entropy generation rate of the system. Also, we unveil through this study that changes in the electroosmotic parameter $\bar{\kappa}$ (representative of the EDL thickness) or the composition of the fluid (ϕ , the volume fraction of nanoparticles agglomerates) non trivially alter the optimum values of these parameters. Inferences drawn from this analysis may have consequences in the optimum design of thermal systems/devices, typically used for thermal management in micro-heat exchangers, micro-reactors, and micro heat pipes.

Keywords Nanofluid · Microfluidic channel · Ionic liquids · Entropy · Electroosmotic transport

List of symbols

Bi	Biot number	k_B	Boltzmann constant
Br	Brinkman number	k	Thermal conductivity ($\text{W m}^{-1} \text{s}^{-1}$)
C_p	Specific heat at constant pressure ($\text{J kg}^{-1} \text{K}^{-1}$)	\bar{k}	Thermal conductivity ratio ($= k_{\text{nf}}/k_f$)
d	Channel wall thickness (m)	L	Channel length (m)
e	Elementary electronic charge ($= 1.6022 \times 10^{-19} \text{C}$)	n_∞	Bulk concentration of ions
E_x	Applied electric field strength ($= \text{V m}^{-1}$)	p	Pressure (Pa)
G	Dimensionless axial temperature gradient ($= \partial\theta/\partial x$)	Pe	Peclet number
H	Half height of the channel (m)	$\langle \dot{S} \rangle$	Dimensionless volumetric entropy generation rate
h	External convective heat transfer coefficient ($= \text{W m}^{-2} \text{K}^{-1}$)	T	Temperature (K)
J	Dimensionless Joule heating parameter	u	Axial velocity (m s^{-1})
		\bar{u}	Dimensionless axial velocity
		U_{HS}	Helmholtz-Smoluchowski velocity (m s^{-1})
		W	Channel width (m)
		x, y	Dimensional axial and transverse coordinates, respectively (m)
		z	Ionic valence

✉ Pranab Kumar Mondal
mail2pranab@gmail.com; pranabm@iitg.ac.in

¹ Department of Mechanical Engineering, Indian Institute of Technology Guwahati, Guwahati 781039, India

² Fluid Mechanics Thermal Engineering and Multiphase Flow Research Laboratory (FUTURE), Department of Mechanical Engineering, Faculty of Engineering, King Mongkut's University of Technology Thonburi, Bangmod, Bangkok 10140, Thailand

Greek symbols

γ	Dimensionless thermal conductivity of wall
δ	Dimensionless channel wall thickness
ε	Dielectric constant of electrolyte ($= \text{F m}^{-1}$)
Θ	Dimensionless temperature

κ	Reciprocal of the characteristic EDL thickness (= m^{-1})
$\bar{\kappa}$	Dimensionless Debye–Hückel parameter
λ_D	EDL thickness (m)
μ	Dynamics viscosity ($\text{kg m}^{-1} \text{s}^{-1}$)
$\bar{\mu}$	Fluid viscosity ratio (= μ_{nf}/μ_f)
ρ	Density (kg m^{-3})
ρ_e	Total ionic charge density inside the EDL (= C m^{-3})
ϕ	Nanoparticle volume fraction
ψ	Electrostatic potential inside EDL

Subscripts

a	Ambient
f	Base fluid
i (= 1, 2)	Lower and upper wall
nf	Nanofluid
np	Nanoparticle
opt	Optimum
s	Wall

Introduction

One branch of microfluidics shows prodigious promise for potential applications in cooling in microscale thermal management systems/devices, in particular, in the micro-electromechanical system (MEMS). With the advancement of technology, several effective ways of cooling of the micro-devices/systems have been proposed by the researchers in recent years [1–6]. One of the available methods relies on the use of nanoparticles in the base fluid as a coolant [5–12]. These small particles have high-thermal conductivity and consequently, increase the heat transfer rate in the associated process [8, 11, 13, 14]. It is important to mention here that the addition of nanoparticles to the base fluid makes it inhomogeneous, which at times alters the underlying thermo-hydrodynamics non-trivially [12, 15, 16]. It is needless to mention that the higher thermodynamic irreversibility generated in the underlying process destroys the exergetic efficiency of the system [17]. The analysis of entropy generation therefore appears to be a convenient tool to assess the intrinsic irreversibilities associated with a microfluidic system and to determine the optimized operating conditions leading to minimum dissipation.

Albeit intuitive, we would like to mention here that several inevitable factors involved with the underlying thermo-electro-hydrodynamics like heat transfer due to finite temperature difference, dissipative effect, and Joule heating effect invite thermodynamic irreversibility in the process and results in irreversible losses of the available energy [18–22]. In the paradigm of microscale transport, flow actuation by applied pressure gradients many a time encounters

difficulties owing to miniaturization of the platform, and at times, the dissipative effects become significant on account of significant frictional losses [2, 22–26]. On the contrary, manipulation of flows in a microfluidic channel using an external electric field has gained humongous popularity owing to a few important encouraging characters like noise-free operation, ease in manipulation, finer controllability, etc. [27, 28]. However, it is important to note that the inevitable Joule heating effect associated with the purely electrically actuated transport leads to entropy generation appreciably. It deteriorates the exergetic efficiency by destroying the available work in the process [3, 4, 29]. Taking a note on these aspects, researchers have considered the combined effects of applied pressure gradient and electrokinetic influence to manipulate flows in the microfluidic environment, essentially to keep the Joule heating and dissipation effects within a manageable limit [3, 30, 31].

It may be mentioned here that several issues associated with the underlying thermo-hydrodynamics as well as thermo-electro-hydrodynamics of nanofluids (nanoparticles mixed with a base fluid) in microscale thermal management systems/devices have been reported by numerous researchers [5–7, 22, 23, 32–37]. In these published works, researchers have shown the promising potential of nanofluids in recovering higher heat as compared to the other coolants. Note that all the systems/devices used for convective transport of heat even in the miniaturized platform have a finite thickness. The conductive transport of heat through bounding surfaces becomes, many times, indispensable to be taken into account on the underlying microscale thermo-hydrodynamics. Simultaneous effects of heat conduction through the bounding surfaces in tandem with the convection of heat through the fluid layer (often called as conjugate heat transfer) bear a significant impact on the thermodynamic efficiency of the microsystems/devices [2, 31, 38, 39]. Paying attention to all these aspects, efforts have been directed at the minimization of system entropy generation towards the optimization of design parameters (both geometric as well as thermophysical) for which thermodynamic performance becomes maximum [21, 39–44]. To the best of authors' knowledge, this aspect has not been explored in the literature to date.

Here, we investigate the transport of a nanofluid through an asymmetrically heated microfluidic channel having finite wall thickness. We consider the combined influences of applied pressure gradient and applied electric field strength for the transportation of the nanofluid through the channel. Considering the effects of viscous dissipation, Joule heating, and conjugate transport of heat, we focus on the entropy generation minimization of this system. Through this analysis, we have shown that the global entropy generation rate of the system displays minimum values when explored as a function of the design parameters, viz. channel wall thickness ratio, Biot number, wall to fluid thermal conductivity

ratio, and Peclet number. Thus, there exist specific conditions for the geometrical and thermophysical parameters which must be taken care of in the design of heat transfer devices for their optimum performance. These parameters determine the optimal working conditions in the sense that the intrinsic irreversibilities become minimum consistent with the physical restrictions of the system and leads to the maximum exergetic efficiency of the system.

Mathematical formulation

Problem description

We consider here, the combined pressure and electroosmotically driven thermofluidic transport of a nanofluid comprising of alumina (Al_2O_3) as the nanoparticle and ionic aqueous solution (aqueous electrolyte) as the base fluid. This steady, unidirectional flow $u = (u(y), 0, 0)$, is taking place through a microfluidic channel formed between two parallel plates. The length, width, and height of the channel are L , W and $2H$, respectively, such that $L \gg W > 2H$ as shown in Fig. 1. This assumption ensures a unidirectional flow under

the applied external forcings. The underlying transport process is considered to be fully developed, both thermally and hydro dynamically. Taking a note on the practical relevance of this study, we consider different but finite thickness for each plate: d_1 for the bottom plate and d_2 for the top one. In this transport process, since an ionic solution is exposed to the solid plates, the surface of each plate becomes charged following an electrostatic interaction between the charged surface and electrolytic solution, and thus, a thin layer of counter ions forms in the interfacial region. This layer is referred to as the electrical double layer (EDL) [45–47]. In this study, we consider the EDLs to be thin and non-overlapping. However, the effect of the Joule heating, invariably present with the EOF of colloidal suspensions, is considered for the current thermofluidic transport process.

Thermophysical properties of nanofluid

We here make an effort to discuss the effective thermophysical properties of nanofluids. Several studies reported in the literature have attempted to discuss the mechanism of enhanced transport of nanoscale colloidal suspensions from the perspective of continuum-based formulation of the

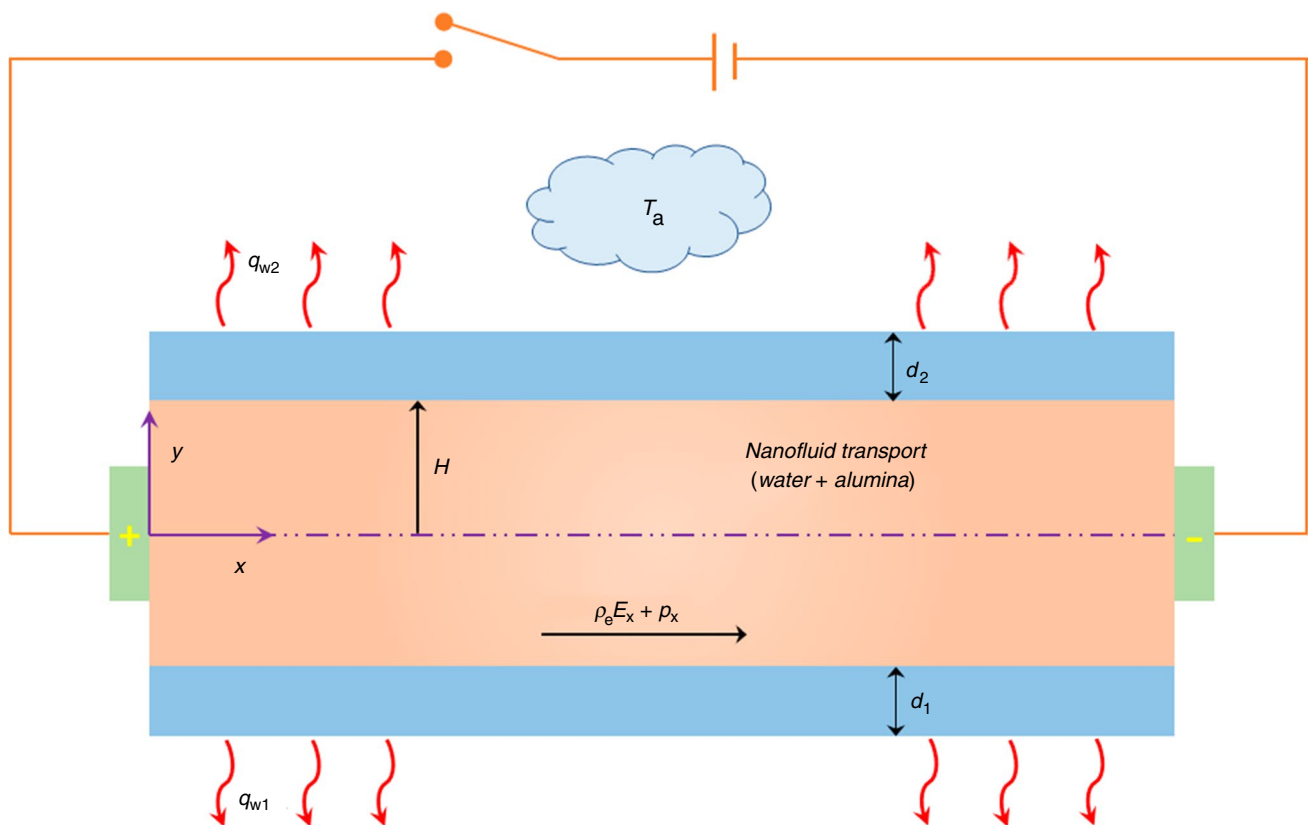


Fig. 1 Schematic depicting the combined pressure driven and electroosmotically actuated thermofluidic transport of a nanofluid through a microchannel formed between two asymmetrically cooled parallel

plates, for which L is the length, W is the width, and $2H$ is the height of the channel

thermophysical properties of nanofluids [9]. To be precise, most of the studies have reported that factors like particle clustering, Brownian motion of the particles, and molecular layering at the fluid-particle interface enhance transport, accounting alteration of the effective thermophysical properties of nanofluid [8, 10]. In addition to these factors, there are several other issues like complex hydrodynamic interactions at small scale and the interparticle interactions, which need to be put in perspective for calculating the effective rheological behaviour and thermophysical properties of nanofluids. These factors stimulate the aggregation of nanoparticles suspended in the base fluid and allow the cluster formation. In this study, we calculate the effective properties of nanofluids from the perspective of continuum-based approach, where the effective viscosity and density of the nanofluid are given by the following relations as written below [16–18]. Also, for the expression of effective density and heat capacitance, we are using the model [32] which can be expressed as:

$$(\rho C_p)_{\text{nf}} = (1 - \phi)(\rho C_p)_f + \phi(\rho C_p)_{\text{np}} \quad (1)$$

where ρ is the density (kg m^{-3}), C_p is the specific heat at constant pressure ($\text{kJ kg}^{-1} \text{K}^{-1}$), and ϕ is the nanoparticle volume fraction. To describe the effective viscosity of the nanofluid, we consider the Brinkman model [11] and following which, the effective dynamic viscosity can be written as:

$$\mu_{\text{nf}} = \mu_f(1 - \phi)^{-5/2} \quad (2)$$

where μ_{nf} is the viscosity of nanofluid, μ_f is the viscosity of the base fluid, and ϕ is the volume fraction. The effective thermal conductivity of the nanofluid is approximated by the Maxwell–Garnett's model and given by [21]:

$$\frac{k_{\text{nf}}}{k_f} = \frac{(k_{\text{np}} + 2k_f) - 2\phi(k_f - k_{\text{np}})}{(k_{\text{np}} + 2k_f) + \phi(k_f - k_{\text{np}})} \quad (3)$$

These thermophysical properties are assumed to remain invariant of temperature in this analysis.

Governing equations for electro-hydrodynamics

For the problem under present consideration, the governing transport equations are the continuity equation, Navier–Stokes equation for the velocity field, and the Poisson–Boltzmann equation for the electrostatic charge distribution [38, 48, 49].

Continuity equation:

$$\frac{du}{dx} = 0 \quad (4)$$

Momentum equation:

Considering the assumptions pertaining to this analysis, the momentum transport equation can be written in the following form:

$$-\frac{dp}{dx} + \mu_{\text{eff}} \frac{d^2 u}{dy^2} + \rho_e E_x = 0 \quad (5)$$

where ρ_e is the total ionic charge density inside the electric double layer (EDL) [45] and E_x is the applied electric field [29, 45, 50]. The EDL charge density ρ_e can be obtained from the Poisson–Boltzmann equation [45] as:

$$\rho_e = -\varepsilon \frac{d^2 \psi}{dy^2} \quad (6)$$

where ψ is the electrostatic potential within the EDL and ε is the dielectric constant of electrolyte. Now, for a z:z symmetric electrolyte, the net ionic charge density is given by [45]

$$\rho_e = ze(n^+ - n^-) \quad (7)$$

here n^+ and n^- are the densities of positive and negative ions, respectively. For the low Reynolds number flow, we can neglect the convection of ions in the microchannel. In this case, we appeal to the Boltzmann distribution to obtain ionic densities for both positive and negative ions, given by [45, 51–54]:

$$n^\pm = n_\infty \exp[\mp(z e \psi)/k_B T] \quad (8)$$

where n_∞ is the bulk concentration of ions, z is the ionic valence, e is the electric charge, T is the absolute temperature of the system, and k_B is the Boltzmann constant. The following two assumptions are now considered for this analysis: (a) the zeta potential is temperature independent and (b) the value of zeta potential is less than 25 mV [45, 55–57]. On the basis of the abovementioned assumptions, we can now apply the Debye–Hückel approximation [38, 58], which linearizes the exponential form of the Boltzmann distribution. Thus, Eq. (6) now takes the form:

$$\frac{d^2 \psi}{dy^2} = \left(\frac{1}{\lambda_D}\right)^2 \psi = \kappa^2 \psi \quad (9)$$

where λ_D is the EDL thickness and $\kappa (= 1/\lambda_D)$ is the Debye–Hückel parameter. It may be mentioned in this context that the magnitude of electroosmotic body force for a given magnitude of applied electric field acting on the fluid mass will depend upon κ [45]. Below we write the boundary conditions employed in this analysis to solve the transport Eqs. (5) and (9).

For the velocity field

$$\left. \begin{aligned} \text{No slip condition at the walls : } & u|_{y=\pm H} = 0 \\ \text{Symmetry at the centre line : } & du/dy|_{y=0} = 0 \end{aligned} \right\} \quad (10)$$

For the electric potential

$$\left. \begin{aligned} \text{At the symmetric plane : } & d\psi/dy|_{y=0} = 0 \\ \text{Specified potential at wall : } & \psi|_{y=\pm H} = \psi_w \end{aligned} \right\} \quad (11)$$

After imposing the boundary condition as delineated in Eq. (11) on Eq. (9) and considering the ionic charge density from Eq. (8), we can rewrite the Eq. (5) as:

$$-\frac{dp}{dx} + \mu_{\text{eff}} \frac{d^2u}{dy^2} - (\epsilon E_x \psi_w \kappa^2) \frac{\cosh(\kappa y)}{\cosh(\kappa H)} = 0. \quad (12)$$

Nondimensionalization of momentum equation

Equation (12) can be non-dimensionalized using the following dimensionless parameters: $\bar{y} = y/H$, $\bar{u} = u/U_{\text{HS}}$, and $\bar{\kappa} = \kappa H (= H/\lambda_D)$. Note that U_{HS} is the Helmholtz-Smoluchowski velocity and is expressed as $U_{\text{HS}} (= -\epsilon E_x \psi_w / \mu_f)$. $\bar{\kappa}$ is the non-dimensional Debye-Hückel parameter. Also, we define a parameter that relates the relative strength of the applied pressure gradient to the electroosmotic excitation strength as $\bar{p}_x = -H^2(dp/dx) / \mu_f U_{\text{HS}}$. Using these non-dimensional parameters, the dimensionless transport equation reads as:

$$\frac{d^2\bar{u}}{d\bar{y}^2} + \left(\frac{\bar{\kappa}}{\sqrt{\mu_{\text{eff}}/\mu_f}} \right)^2 \frac{\cosh(\bar{\kappa}\bar{y})}{\cosh(\bar{\kappa})} + \bar{p}_x = 0 \quad (13)$$

where $\bar{\mu} = \mu_{\text{eff}}/\mu_f$ is the fluid viscosity ratio or relative viscosity of nanofluid and carrier fluid [24], and $\bar{p}_x = p_x \mu_f / (\mu_{\text{eff}})$ is the modified pressure gradient parameter.

The boundary condition for velocity in dimensionless form

$$\text{No slip boundary condition at the channel walls : } \bar{u}|_{\bar{y}=\pm 1} = 0 \quad (14)$$

$$\text{Maximum velocity at the centre line due to symmetry : } d\bar{u}/d\bar{y}|_{\bar{y}=0} = 0 \quad (15)$$

Utilizing the boundary conditions given in Eqs. (14)–(15), we can find the non-dimensional velocity profile solving Eq. (13). The expression for dimensionless flow velocity reads:

$$\bar{u} = \frac{1}{\bar{\mu}} \left[1 - \frac{\cosh(\bar{\kappa}\bar{y})}{\cosh(\bar{\kappa})} \right] + \frac{\bar{p}_x}{2} (1 - \bar{y}^2) \quad (16)$$

For the brevity in presentation, we recast Eq. (16) in the following form:

$$\bar{u} = g_1 \cosh(\bar{\kappa}\bar{y}) + g_2 \bar{y}^2 + g_3 \quad (17)$$

where $g_1 = (-\text{sech}(\bar{\kappa})/\bar{\mu})$, $g_2 = (-\bar{p}_x/2)$ and $g_3 = [(1/\bar{\mu}) + (\bar{p}_x/2)]$.

Governing equation for temperature distribution

The governing equation describing the thermal energy transport associated with the flow of nanofluid inside the micro-channel (considering axial conduction, viscous dissipation, and volumetric heat generation terms) can be expressed as:

$$(\rho C_p)_{\text{nf}} u \frac{\partial T}{\partial x} = k_{\text{eff}} \left(\frac{\partial^2 T}{\partial y^2} \right) + \mu_{\text{eff}} \left(\frac{du}{dy} \right)^2 + \sigma E_x^2 \quad (18)$$

where ρ_{nf} is the density of nanofluid, E_x is the applied electric field, and σ is the charge density. Note that, the second and third terms on the right-hand side of Eq. (18) take into account the viscous dissipation and Joule heating effects, respectively. Furthermore, to take the effect of conjugate heat transfer into the underlying analysis, we consider the following energy equation for both the walls of the channel:

$$\frac{d^2 T_{\text{si}}}{dy^2} = 0 \quad (19)$$

where T_{si} is the wall temperature ($i = 1, 2$ indicate the lower and upper walls, respectively). To solve the energy transport equations in the solid walls as well as in the flow field, we consider the following set of boundary conditions [31]: Temperature continuity at the fluid-wall interface:

$$\left. \begin{aligned} T|_{y=-H} &= T_{s1} \\ T|_{y=+H} &= T_{s2} \end{aligned} \right\} \quad (20)$$

Heat flux continuity at the fluid-wall interface:

$$\left. \begin{aligned} k_{\text{eff}}(dT/dy)|_{y=-H} &= k_{s1}(dT_{s1}/dy) \\ k_{\text{eff}}(dT/dy)|_{y=+H} &= k_{s2}(dT_{s2}/dy) \end{aligned} \right\} \quad (21)$$

where k_{s1} and k_{s2} are the thermal conductivities of the lower and upper walls, respectively.

Convective boundary conditions at the outer surface of upper and lower walls:

$$\left. \begin{aligned} k_{s1}(dT_{s1}/dy)|_{y=-(H+d_1)} &= h_1(T_{s1} - T_a) \\ k_{s2}(dT_{s2}/dy)|_{y=+(H+d_2)} &= h_2(T_{s2} - T_a) \end{aligned} \right\} \quad (22)$$

where h_1 and h_2 are the heat transfer coefficient of the ambient fluid at the lower and upper wall of the microchannel, respectively.

Non-dimensionalisation of energy equations

To non-dimensionalize the energy Eqs. (18) and (19), we consider the following dimensionless parameters: $\bar{x} = x/H$, $\bar{y} = y/H$, $\bar{u} = u/U_{HS}$, $\Theta_{si} = (T - T_a)/\Delta T_j$, $\Theta_a = T_a/\Delta T_j$, $\delta_1 = d_1/H$, and $\delta_2 = d_2/H$, where $\Delta T_j = (\sigma E_x^2 H^2 / k_{eff})$ is the characteristics change in temperature due to Joule heating effect. Θ is the dimensionless fluid temperature, Θ_{si} ($i = 1, 2$) is the dimensionless wall temperature, and Θ_a is the dimensionless ambient temperature. Substituting these dimensionless parameters into Eqs. (18) and (19), we get the dimensionless energy equation in the flow field as [38]:

$$\overline{Pe} \bar{u} \frac{\partial \Theta}{\partial \bar{x}} = \frac{\partial^2 \Theta}{\partial \bar{y}^2} + \overline{Br} \left(\frac{d\bar{u}}{d\bar{y}} \right)^2 + \bar{J} \quad (23)$$

To mention, the dimensionless energy equation in solid walls reads as [38]:

$$\frac{d^2 \Theta_{si}}{d\bar{y}^2} = 0 \quad (24)$$

A few dimensionless parameters appearing in Eq. (23) are described as follows: The Peclet number: $Pe = (HU_{HS}(\rho C_p)_f) / k_f$, Brinkman number: $Br = (\mu_f U_{HS}^2 / k_f \Delta T_j)$, Joule heating parameter: $J = (\sigma H^2 E_x^2) / k_f \Delta T_j$ and $\bar{k} = k_{eff} / k_f$ is the thermal conductivity ratio. Also, we define the following modified parameters pertinent to this analysis as: $\overline{Pe} = Pe(\rho C_p)_{nf} / \bar{k}(\rho C_p)_f$ is the modified Peclet number, $\overline{Br} = Br / (\bar{k} / \bar{\mu})$ is the modified Brinkman number, and $\bar{J} = J / \bar{k}$ is the modified Joule heating parameter. The dimensionless counterpart of the boundary conditions delineated in Eqs. (20)–(22) can be written in the following form:

Temperature continuity at the fluid–wall interface:

$$\begin{aligned} \Theta|_{\bar{y}=-1} &= \Theta_{s1} \\ \Theta|_{\bar{y}=+1} &= \Theta_{s2} \end{aligned} \quad (25)$$

Heat flux continuity at the fluid–wall interface:

$$\begin{aligned} (d\Theta/d\bar{y})|_{\bar{y}=-1} &= \gamma_1 (d\Theta_{s1}/d\bar{y}) \\ (d\Theta/d\bar{y})|_{\bar{y}=+1} &= \gamma_2 (d\Theta_{s2}/d\bar{y}) \end{aligned} \quad (26)$$

where the wall thermal conductivity ratio $\gamma_i = (k_{si} / k_{eff})$ is the ratio between the thermal conductivities of wall and nanofluid, (here $i = 1, 2$ stands for the lower and upper wall, respectively).

Convective boundary conditions at the outer surface of the channel walls

$$\begin{aligned} (d\Theta_{s1}/d\bar{y})|_{\bar{y}=-(1+\delta_1)} &= Bi_1 (\Theta_{s1} - \Theta_a) \\ (d\Theta_{s2}/d\bar{y})|_{\bar{y}=+(1+\delta_2)} &= Bi_2 (\Theta_{s2} - \Theta_a) \end{aligned} \quad (27)$$

Note that $Bi_i (= h_i H / k_{si})$ in Eq. (27) is the Biot number and signifies the ratio of heat convection at the surface of the microchannel to heat conduction in the walls of the channel. As mentioned earlier, our attention in this investigation is centered on the thermally fully developed transport under steady but unequal heat flux boundary conditions. Considering this aspect, we can compose the dimensionless temperature in the accompanying forms [59]:

$$\Theta = G\bar{x} + \theta(\bar{y}) \quad (28)$$

It is important to mention here that G in Eq. (28) signifies the axial temperature gradient and considered to remain constant in this analysis. Now, solving the energy transport Eq. (23) using the temperature profile given in Eq. (28), we get the temperature distribution in the flow field. Below we write the dimensionless temperature distribution in the flow field as:

$$\begin{aligned} \theta &= g_4 \cosh(\bar{k}\bar{y}) - g_5 \cosh(2\bar{k}\bar{y}) + g_6 \bar{y}^4 + g_7 \bar{y}^2 \\ &\quad - g_8 \bar{y} \sinh(\bar{k}\bar{y}) + C_1 \bar{y} + C_2 \end{aligned} \quad (29)$$

where C_1 and C_2 are the constants yet to be determined. The mathematical expressions for the coefficients $g_4 - g_8$ appearing in Eq. (29) are written below for the sake of completeness.

$$g_4 = \left[\left(\overline{Pe} G g_1 / \bar{k}^2 \right) + \left(2\overline{Br} X_3 / \bar{k}^3 \right) \right]$$

$$g_5 = \left(\overline{Br} X_1 / 8\bar{k}^2 \right)$$

$$g_6 = \left[\left(\overline{Pe} G g_2 / 12 \right) - \left(\overline{Br} X_2 / 12 \right) \right]$$

$$g_7 = \left[\left(\overline{Pe} G g_3 / 2 \right) + \left(\overline{Br} X_1 / 4 \right) - \left(\bar{J} / 2 \right) \right];$$

$$g_8 = \left(\overline{Br} X_3 / \bar{k}^2 \right)$$

$$X_1 = (g_1 \bar{k})^2$$

$$X_2 = (2g_2)^2$$

$$X_3 = (4g_1 g_2 \bar{k})$$

Now, solving Eq. (24), for the wall temperatures, we get

$$\left. \begin{aligned} \theta_{s1} &= C_3\bar{y} + C_4 \\ \theta_{s2} &= C_5\bar{y} + C_6 \end{aligned} \right\} \tag{30}$$

where $C_3 - C_6$ are the constants. Using the boundary conditions mentioned in Eqs. (26)–(28), we evaluate the constants $C_1 - C_6$ appearing in Eqs. (29), (30) as follows:

$$C_1 = \frac{X_4[\gamma_2 Bi_2(1 + \delta_1 Bi_1) - \gamma_1 Bi_1(1 + \delta_2 Bi_2)]}{(4\gamma_1\gamma_2 Bi_1 Bi_2) + 2\gamma_2 Bi_2(1 + \delta_1 Bi_1) + 2\gamma_1 Bi_1(1 + \delta_2 Bi_2)}$$

$$C_3 = \frac{(-X_4 Bi_1)(1 + \gamma_2 Bi_2 + \delta_2 Bi_2)}{(2\gamma_1\gamma_2 Bi_1 Bi_2) + \gamma_2 Bi_2(1 + \delta_1 Bi_1) + \gamma_1 Bi_1(1 + \delta_2 Bi_2)}$$

$$C_4 = \frac{-X_4(1 + \gamma_2 Bi_2 + \delta_2 Bi_2)(1 + Bi_1 + \delta_1 Bi_1)}{(2\gamma_1\gamma_2 Bi_1 Bi_2) + \gamma_1 Bi_1(1 + \delta_2 Bi_2) + \gamma_2 Bi_2(1 + \delta_1 Bi_1)} + \theta_a$$

$$C_5 = \frac{X_4 Bi_2(1 + \delta_1 Bi_1 + \gamma_1 Bi_1)}{(2\gamma_1\gamma_2 Bi_1 Bi_2) + \gamma_1 Bi_1(1 + \delta_2 Bi_2) + \gamma_2 Bi_2(1 + \delta_1 Bi_1)}$$

$$C_6 = \frac{-X_4(1 + \delta_1 Bi_1 + \gamma_1 Bi_1)(1 + Bi_2 + \delta_2 Bi_2)}{(2\gamma_1\gamma_2 Bi_1 Bi_2) + \gamma_1 Bi_1(1 + \delta_2 Bi_2) + \gamma_2 Bi_2(1 + \delta_1 Bi_1)} + \theta_a$$

$$C_2 = C_1 - C_3 + C_4 + X_5$$

where

$$\left. \begin{aligned} X_4 &= 2\bar{\kappa}g_4 \sinh(\bar{\kappa}) - 4\bar{\kappa}g_5 \sinh(2\bar{\kappa}) + 8g_6 + 4g_7 - 2g_9[\bar{\kappa} \cosh(\bar{\kappa}) + \sinh(\bar{\kappa})] \\ X_5 &= g_4 \cosh(\bar{\kappa}) - g_5 \cosh(2\bar{\kappa}) + g_6 + g_7 - g_8 \sinh(\bar{\kappa}) \end{aligned} \right\} \tag{31}$$

The aforementioned constants are used to obtain the temperature distribution for this conjugate heat transfer problem.

The entropy generation rate of the system

Entropy generation of a system is calculated by measuring its thermodynamic irreversibilities. Note that the thermal systems/devices encounter thermodynamic irreversibility largely stemming from the momentum and energy exchange phenomena involved with the underlying thermo-fluidic transport. For any thermodynamic framework, the minimization of the entropy generation is essential for obtaining the best exergetic efficiency. To mention, for the problem under the present consideration, the irreversible losses emerge from the following three sources, to be specific, heat transfer because of the finite temperature difference, inevitable Joule heating effect due to electroosmotic effect and the viscous dissipation [20]. The general articulation for the volumetric

entropy generation rate [19] in the dimensional structure can be composed as [18, 40, 49, 60–64]:

$$\begin{aligned} S_g &= \frac{k_{\text{eff}}}{T^2} \left[\left(\frac{\partial T}{\partial x} \right)^2 + \left(\frac{\partial T}{\partial y} \right)^2 \right] + \frac{k_{s1}}{T_{s1}^2} \left(\frac{\partial T_{s1}}{\partial y} \right)^2 \\ &+ \frac{k_{s2}}{T_{s2}^2} \left(\frac{\partial T_{s2}}{\partial y} \right)^2 + \frac{\mu_{\text{eff}}}{T} \left(\frac{du}{dy} \right)^2 + \frac{\sigma E_x^2}{T} \end{aligned} \tag{32}$$

In this expression, it can be seen that four different factors are responsible for entropy generation in the present problem. The first-term in the above equation brings up the temperature gradient in the nanofluid. In contrast, the second and third terms are also showing the effect of temperature gradient but in the lower and upper walls of the microchannel, respectively. The fourth term in Eq. (32) represents the volumetric viscous dissipation in the microchannel, while the final term takes care of the irreversibility associated with the Joule heating effect. Below we write the dimensionless form of Eq. (32) that reads as:

$$\begin{aligned} \dot{S} &= \frac{1}{\Theta^2} \left[\left(\frac{\partial \Theta}{\partial \bar{x}} \right)^2 + \left(\frac{\partial \Theta}{\partial \bar{y}} \right)^2 \right] + \frac{\gamma_1}{\Theta_{s1}^2} \left(\frac{\partial \Theta_{s1}}{\partial \bar{y}} \right)^2 \\ &+ \frac{\gamma_2}{\Theta_{s2}^2} \left(\frac{\partial \Theta_{s2}}{\partial \bar{y}} \right)^2 + \frac{\overline{\text{Br}}}{\Theta} \left(\frac{d\bar{u}}{d\bar{y}} \right)^2 + \frac{\bar{J}}{\Theta} \end{aligned} \tag{33}$$

here $\dot{S} = S_g H^2 / k_{\text{eff}}$ is the non-dimensional volumetric entropy generation rate. For the evaluation of the optimum value of system parameters, which is the prime objective of this study, the overall entropy generation rate in the sys-

tem is required. Accordingly, we have made an effort in this analysis to achieve the overall entropy generation rate per unit length in the axial direction, i.e. $\langle \dot{S} \rangle$. In doing so, we perform numerical integration of the expression, delineated in Eq. (33), within the system volume.

Model Validation

In this section, we make an effort to validate our theoretical model by comparing the results with the experimental results of electroosmotic transport in a microfluidic channel. In doing so, we show in Fig. 2, the velocity distribution in the transverse direction of the channel. Note that the results obtained from our theoretical analysis (shown by a solid line) are compared with the reported experimental results (indicated by ‘o’ marker) of Hsieh and Yang [65]. Having a closer look at Fig. 2, it can be inferred that our analytical results match well with the experimental results

reported by Hsieh and Yang [65]. This supports the efficacy of our theoretical model uses in this analysis. Note that the other parameters considered for plotting Fig. 2 confirm to those as reported in Ref. [65]. Also, we show in Fig. 2b, the variation of flow velocity for four different values of $\bar{\kappa}$ ($= 15, 20, 25$ and 35). As seen in Fig. 2b, the flow velocity as well as its gradient increases inside the EDL with an increasing value of $\bar{\kappa}$. With increasing $\bar{\kappa}$, the EDL becomes thinner, and this layer squeezes more number of counter ions (ionic density in the EDL becomes higher). Upon interacting with the external electric field, these ions experience relatively stronger electroosmotic body force. Thus, the electroosmotic body force, which is acting on the fluid mass in the EDL, becomes higher for a higher value of $\bar{\kappa}$, leading to an enhancement in flow velocity, as seen from Fig. 2b.

Results and discussion

Selection of parameters

In this section, we analyze the consequences of conjugate transport of heat, Joule heating effect, and viscous dissipation on the entropy generation rate associated with the field-driven transport of nanofluid in a microfluidic channel. As such, to get insights about the entropy generation rate in the system considered in the present analysis, we depict some parametric variations which include the thermophysical

as well as geometrical parameters such as Peclet number (Pe), lower wall thermal conductivity ratio (γ_1), lower wall thickness ratio (δ_1), and lower wall Biot number (Bi_1). In this analysis, since the interfacial electro-chemistry enacts a crucial role in the underlying transport, we aspire for the variation for different values of Debye–Hückel parameter ($\bar{\kappa}$), the volume fraction of nanoparticle (ϕ), and Joule heating parameter (J), respectively. Complying with the prime focus of this analysis, we look at the optimum value of the aforementioned parameters (both geometrical and thermo-physical) to ensure a minimum entropy generation rate in the system. Also, unless specified otherwise, we have considered the following set of parameters in this analysis as follows: $\Theta_a = 5$ (dimensionless ambient temperature), $\delta_1 = \delta_2 = 0.1$, $p_x = 1$, $Br = 0.1$, $J = 1$, $Bi_1 = 1$, $Bi_2 = 5$, $Pe = 0.1$, $\gamma_1 = 1$, $\gamma_2 = 1$, and $G = 1$ (axial temperature gradient). Note that the considered value of the aforementioned parameters is typical to microscale transport and has been reported in the literature [65].

Entropy generation

Effect of lower wall thickness ratio (δ_1) on the system irreversibility

In Fig. 3a, b, we depict the variation of normalized global entropy generation $\langle \dot{S} \rangle / \langle \dot{S} \rangle|_{\delta_1=0}$ against lower wall thick-

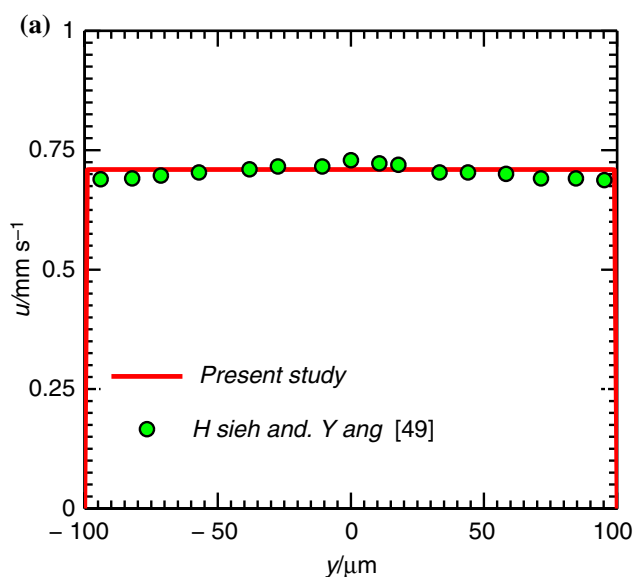
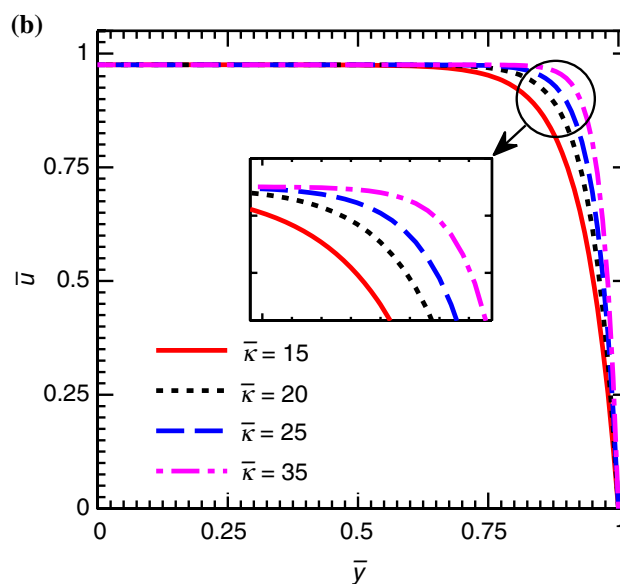


Fig. 2 a Validation: plot showing the variation of axial velocity in the transverse direction of the channel. The plot shown by the solid line is obtained from the present theoretical analysis, while the variation indicated by marker ‘o’ indicates the results reported by Hsieh and Yang [65]. The other parameters considered for this plotting are: $E_x = 15 \text{ KV } m^{-1}$, $\kappa = 1.06 \text{ nm}^{-1}$, $\epsilon = 644.47 \times 10^{-12} \text{ Fm}^{-1}$,



$\mu_f = 803.4 \times 10^{-6} \text{ Pa s}$, and $H = 100 \text{ } \mu\text{m}$; **b** plot of velocity distribution in the channel, obtained for four different values of $\bar{\kappa}$. The other parameters considered for this plotting are: $\phi = 1\%$, $\bar{\mu} = 1.025$, $p_x = 0$. With the increasing value of $\bar{\kappa}$, both the flow velocity and its gradient becomes higher in the EDL

ness ratio (δ_1), obtained for two different parameters, viz. the Debye–Hückel parameter ($\bar{\kappa}$) and volume fraction of nanofluid (ϕ), respectively. For the variation depicted in Fig. 3a, we have considered three different values of $\bar{\kappa}$ keeping nanoparticle volume fraction (ϕ) constant, while for Fig. 3b nanoparticle volume fraction is varied for a given $\bar{\kappa}$. The other parameters have been mentioned in the caption.

Figure 3a depicts the effect of $\bar{\kappa}$ on the entropy generation rate of the system. Before going to discuss the variation at hand, we would like to mention here that with an increase in $\bar{\kappa}$ the EDL becomes thinner. Thinner the EDL, higher will be the electroosmotic body force being applied on the fluid mass in EDL. Now, experiencing a relatively higher magnitude of electroosmotic body force for higher $\bar{\kappa}$, the flow velocity will increase in the region close to the walls (which is EDL) as confirmed in Fig. 2b. To mention, this phenomenon will lead to an increase in both the magnitude of velocity as well as its gradient inside the EDL (see Fig. 2b). As a result, the viscous dissipation, which is directly proportional to the velocity gradient, will increase near the wall. Notably, this higher dissipation will lead to an increment in the temperature of the system through viscous heating. However, the increment in temperature of the system lowers the irreversibility associated with viscous dissipation effects due to its inverse relationship with the fluid temperature (see Eq. 33). Having a closer look at Fig. 3a, b, one can find that entropy generation behaviour follows a trend as discussed next. Entropy generation rate shows an initial decreasing trend with wall thickness and leaving a minimum value; it increases further as wall thickness increases further. Initial decrement of the global

entropy generation rate with increasing δ_1 ($0 < \delta_1 \leq \delta_{1,\text{opt}}$) can be explained as follows: with increasing δ_1 in the range of $0 < \delta_1 \leq \delta_{1,\text{opt}}$, the conductive transport of heat from the lower plate decreases and results in a simultaneous rise in fluid temperature and drop in entropy generation rate. However, with a further increasing δ_1 in the range of $\delta_1 > \delta_{1,\text{opt}}$, a rise in temperature aggravates the transport of heat through the upper wall and stimulates the system entropy generation rate as can be seen from Fig. 3a. This typical variation leads to an optimum wall thickness for which system entropy generation becomes minimum. From the previous discussion, it can be inferred that the effect of heat conduction through lower wall together with the other auxiliary effects like viscous dissipation and Joule heating take a dominating role for the system entropy generation for $\delta_1 \leq \delta_{1,\text{opt}}$. On the other hand, cumulative effects to upper wall heat conduction and convection of heat from therein become the dominating factor in dictating the system entropy generation rate as the Joule heating and viscous dissipation effects are remaining almost unaffected. The definitive outcome of this effect eventually diminishes the net entropy generation rate of the system for higher values of $\bar{\kappa}$. A critical look at Fig. 3a further restores that with an increase in $\bar{\kappa}$, the global entropy generation decreases and the value of $\delta_{1,\text{opt}}$ also gets increased. As mentioned, higher $\bar{\kappa}$ indicates thinner EDL, and consequently for this higher value of $\bar{\kappa}$, the velocity gradient will increase in the EDL. The higher velocity gradient stimulates the dissipative heat, which in turn, will lower the fluid viscosity. For the relatively higher value of $\bar{\kappa}$, thermodynamic irreversibility associated with the viscous

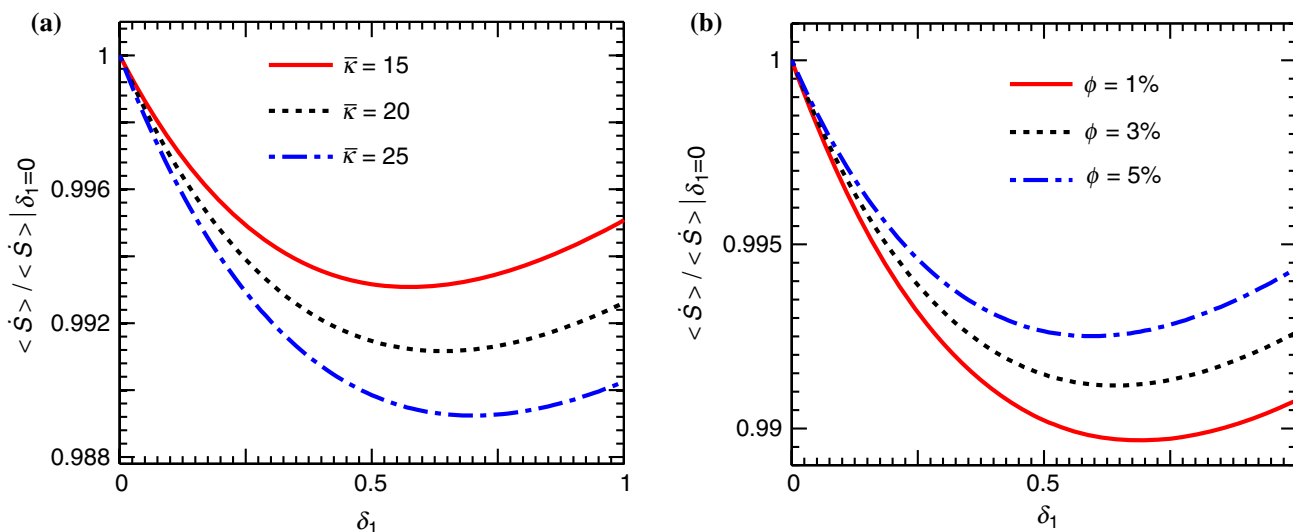


Fig. 3 Disparity of the normalized global entropy generation rate as a function of dimensionless lower wall thickness ratio (δ_1) for **a** $\phi = 3\%$ and different value of $\bar{\kappa}$, **b** $\bar{\kappa} = 20$ and different value of ϕ . Other parameters are considered as $p_x = 1$, $\delta_2 = 0.1$, $\text{Br} = 0.1$,

$J = 1$, $\text{Bi}_1 = 1$, $\text{Bi}_2 = 5$, $\text{Pe} = 0.1$, and $\gamma_1 = \gamma_2 = 1$. The CPU time for $\bar{\kappa} = (15, 20, 25)$ and $\phi = (1, 3, 5)$ are (166.86, 172.2, 181.18) s and (177.92, 172.08, 169.44) s, respectively

dissipation of the present system becomes important as realized by a decrement in global entropy generation in Fig. 4. We attribute this decrement to a drop in fluid viscosity. A little increment in $\delta_{1,\text{opt}}$ with the increasing value of $\bar{\kappa}$ as seen from Fig. 3a as well as to offset the enormous decline in entropy generation associated with viscous dissipation (with increasing $\bar{\kappa}$, drop in fluid temperature results in a decrease in dissipation effect appreciably) with increase in the same in the present scenario.

Figure 3b describes the effect of nanoparticle volume fraction (ϕ) on the entropy generation rate of the system. It can be noted that with increasing ϕ , albeit convective transport of heat increases, the entropy generation of the system increases for every value of δ_1 . Note that with an increasing value of the nanoparticle volume fraction, the effective value of k_{eff} and μ_{eff} increases. This increment in effective thermo-physical properties leads to an enhancement in the entropy generation rate of the system following augmented convective heat transport and the viscous dissipation effect. In Fig. 3b, it has been noted that $\langle \dot{S} \rangle / \langle \dot{S} \rangle|_{\delta_1=0}$ first decreases up to $\delta_{1,\text{opt}}$, attain the lowest value and then increases further as δ_1 increases beyond $\delta_{1,\text{opt}}$. This observation holds good for all the values of ϕ under consideration. We here make an effort to figure out the physical reasoning behind this observation as follows: with the increasing magnitude of δ_1 , the temperature of the fluid and its gradient gets redesigned due to the increased resistance to the conductive transport of heat through the lower wall. In particular, this effect leads to a decrease in the entropy generation rate related to heat

transfer through the lower wall. Regardless, an increase in temperature of the liquid and its gradient builds the heat transfer rate between the liquid and upper wall hence increasing $\langle \dot{S} \rangle$ is the consequential effect, as seen from Fig. 3b. Up to a specific value of δ_1 ($\sim \delta_{1,\text{opt}}$), the decreasing rate of entropy generation dominates over the expansion of $\langle \dot{S} \rangle$ due to the augmented transport of heat in the fluid and upper wall. This results in a net decrease in entropy generation of the structure up to a point $\delta_{1,\text{opt}}$, after which $\langle \dot{S} \rangle$ increases on account of the increase in the irreversibility related to the heat transfer through the liquid and upper wall.

From Eq. (33), it is seen that the global entropy generation of the present system depends upon several factors, viz. convective heat transfer, conductive transport through walls, viscous dissipation, and the Joule heating effects. Now to establish their effects through a quantitative manner, we depict Fig. 4, which shows the contribution of individual effect on the global entropy generation rate. Figure 4 shows that with the increasing value of δ_1 , the entropy generation of the system related to the convective heat transfer through the liquid ($\langle \dot{S} \rangle_{\text{convec.}}$) and conductive heat transfer through the upper wall ($\langle \dot{S} \rangle_{w2}$) increases, while entropy generation related to the conductive heat transfer through the lower wall ($\langle \dot{S} \rangle_{w1}$) decreases. With the increasing value of δ_1 , the temperature of the fluid and its gradient becomes higher due to the reduction in the entropy generation related to the heat transfer through the lower wall. In any case, an increase in temperature of the fluid and its gradient builds the convective heat transfer rate through the fluid and upper wall, as confirmed in Fig. 4. Also, a reduction in heat conduction through the lower wall promotes the conductive transport of heat through the upper wall, as witnessed in Fig. 4. Henceforth, we can presume that in the range $0 < \delta_1 < \delta_{1,\text{opt}}$, the fluid temperature controls the entropy generation rate of the system, while for the range $\delta_1 > \delta_{1,\text{opt}}$, the temperature gradient plays a significant role in deciding the net entropy generation of the present system.

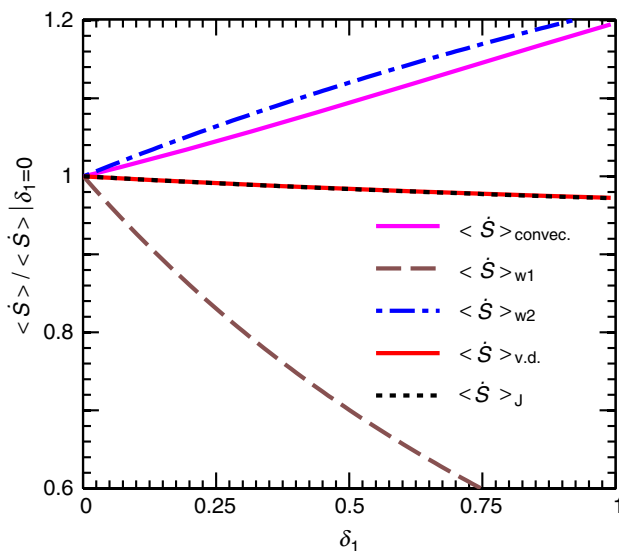


Fig. 4 Disparity of normalized global entropy generation rate of the individual terms associated with Eq. (33) as a function of dimensionless lower wall thickness ratio (δ_1); other parameters: $p_x = 1$, $\delta_2 = 0.1$, $Br = 0.1$, $J = 1$, $Bi_1 = 1$, $Bi_2 = 5$, $Pe = 0.1$, and $\gamma_1 = \gamma_2 = 1$

Effect of thermal conductivity ratio (γ_1) on the system irreversibility

In Fig. 5a, b, we illustrate the variation of normalized global entropy generation $\langle \dot{S} \rangle / \langle \dot{S} \rangle|_{\gamma_1=0}$ versus the lower wall to nanofluid thermal conductivity ratio (γ_1) for three distinct parameters, viz. the Debye–Hückel parameter ($\bar{\kappa}$) and volume fraction of nanofluid (ϕ). Figure 6 portrays the contribution of different terms on the global entropy generation with increasing value of δ_1 . The other parameters considered for plotting the figures have been mentioned in the caption. Next, we discuss the underlying physical reasoning behind the variations as observed from Fig. 5a. Also, to support our argument in explaining the trend, as seen in Fig. 5a, b

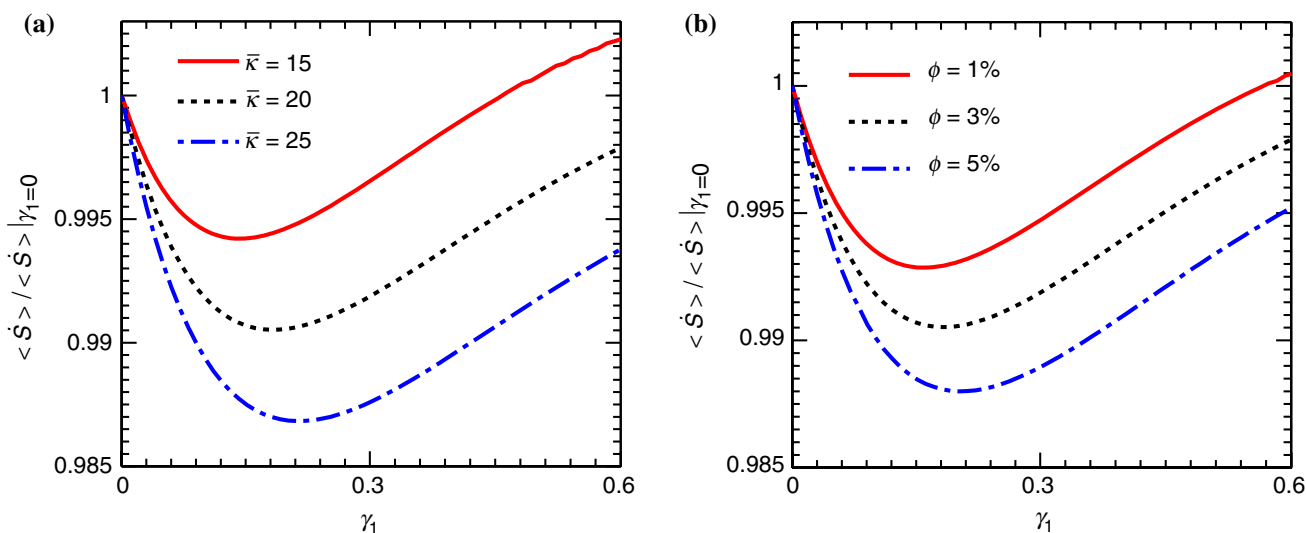


Fig. 5 Disparity of the normalized global entropy generation rate as a function of dimensionless thermal conductivity ratio for lower wall (γ_1); **a** for $\phi = 3\%$ and different value of $\bar{\kappa}$; **b** for $\bar{\kappa} = 20$ and different value of ϕ ; and others data are $p_x = 1, \gamma_2 = 5, Br = 0.1, J = 1,$

$Pe = 0.1, Bi_1 = Bi_2 = 1,$ and $\delta_1 = \delta_2 = 0.1.$ The CPU time for $\bar{\kappa} = (15, 20, 25)$ and $\phi = (1, 3, 5)$ are (153.87, 166.27, 176.9) s and (171.35, 166.3, 161.45) s respectively

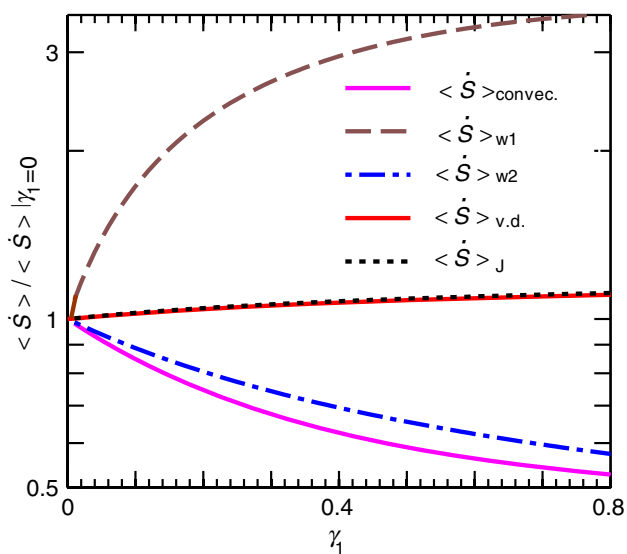


Fig. 6 Disparity of normalized global entropy generation rate of the individual terms associated with Eq. (33) as a function of γ_1 ; other parameters: $p_x = 1, \gamma_2 = 5, Br = 0.1, J = 1, Pe = 0.1, Bi_1 = Bi_2 = 1,$ and $\delta_1 = \delta_2 = 0.1$

through quantitative assessment, we appeal to the variation delineated in Fig. 6.

Figure 5a demonstrates the effect of $\bar{\kappa}$ on the global entropy generation rate of the present system. Here, also, the variation of net entropy generation shows a decreasing-increasing pattern with γ_1 . With an increase in γ_1 , the entropy generation due to heat conduction through lower wall increases as confirmed by the increase in irreversibility

$\langle \dot{S} \rangle_{w1}$ with γ_1 in Fig. 6. An increase in conductive transport of heat with increasing γ_1 results in a reduction in heat transfer associated with the fluid (convective transport) and the upper wall (conductive transport) as witnessed by the decreasing trend of $\langle \dot{S} \rangle_{convec.}$ and $\langle \dot{S} \rangle_{w2}$ in Fig. 6. Important to mention, in the regime of $0 < \gamma_1 \leq \gamma_{1,opt}$, the combined influences of convective heat transport through fluid and conductive transport through the upper wall take a lead role in dictating the global entropy generation in the system as witnessed by the decreasing trend of $\langle \dot{S} \rangle / \langle \dot{S} \rangle_{\gamma_1=0}$ in Fig. 5a, b. However, in the range of $\gamma_1 > \gamma_{1,opt}$, a significant increment in conductive transport of heat through lower wall ($\langle \dot{S} \rangle_{w1}$) together with the favourable effects of nanoparticle driven alteration in viscous dissipation effect and Joule heating (increasing trend of $\langle \dot{S} \rangle_{v.d.}$ and $\langle \dot{S} \rangle_J$ in Fig. 6) leads to a rise in the system entropy generation rate. This observation is realized by an increasing trend of $\langle \dot{S} \rangle / \langle \dot{S} \rangle_{\gamma_1=0}$ in Fig. 5a, b). Thus, we can conclude that in this regime of $\gamma_1 > \gamma_{1,opt}$, conductive transport of heat becomes crucial in dictating the system entropy generation rate. Because of this typical phenomenon of system entropy generation as governed by several influencing factors in different regimes of γ_1 , we observe a decreasing-increasing trend of global entropy generation rate in Fig. 5a, b. It is worth adding here that this decreasing-increasing trend yields an optimum value of γ_1 ($\gamma_{1,opt}$) as seen from Fig. 5a, b.

From Fig. 5a, it can be noticed that with increasing $\bar{\kappa}$, the global entropy generation of the system becomes lesser for all values of γ_1 . Note that with increasing $\bar{\kappa}$, the

electroosmotic body force acting on the fluid mass increases, leading to a rise in velocity gradient in the flow field. This higher velocity gradient increases the dissipative heating and results in a reduction in the temperature gradient between the fluid and walls of the microchannel. The overall phenomenon leads to a reduction in conductive transport of heat, and consequently, the system irreversibility reduces. As discussed before, an increase in ϕ is responsible for an increase in both effective thermal conductivity and effective viscosity of nanofluid. Thus, for a higher volume fraction of nanoparticle (ϕ), the dissipative heat, as well as Joule heating produced becomes higher and results in an increment in fluid temperature. Note that this higher fluid temperature weakens the temperature gradient between the fluid and the walls of the channel. Precisely, a decrease in temperature gradient reduces the heat transfer through the walls and culminating in a reduction in system entropy generation rate, as seen in Fig. 5b. A closer look at Fig. 5b further reveals that with increasing the magnitude of ϕ , the optimum value of γ_1 ($\gamma_{1,\text{opt}}$) increases. This is because of the fact that for higher values of ϕ , the enhancement in viscous dissipation and heat transfer irreversibility at the lower wall counterbalances the reduction in $\langle \dot{S} \rangle$ associated with heat transfer associated irreversibility through the fluid (convective transport) and the upper wall (conductive transport) for a relatively lower value of γ_1 .

Effect of modified Peclet number ($\overline{\text{Pe}}$) on the system irreversibility

We show in Fig. 7a, b, the variation of normalized global entropy generation $\left(\frac{\langle \dot{S} \rangle}{\langle \dot{S} \rangle}|_{\overline{\text{Pe}}=0} \right)$ (normalized with its value when $\overline{\text{Pe}}=0$) rate versus modified Peclet number ($\overline{\text{Pe}}$) for two distinct parameters, viz. the Debye–Hückel parameter ($\bar{\kappa}$) and volume fraction of nanoparticle (ϕ). Note that to obtain the plots depicted in Fig. 7a, we have considered three different $\bar{\kappa}$ ($= 15, 25$ and 35). From the Fig. 7a, b, we observe that with an increase in $\overline{\text{Pe}}$ from 0 to 1.5, the variation of entropy generation shows a decreasing-increasing trend irrespective of the value of $\bar{\kappa}$ and ϕ considered. As such, this typical variation indicates the existence of optimum $\overline{\text{Pe}}$ for all the cases at which the system entropy generation reaches a minimum value.

Also, to figure out the contribution of each term in Eq. (33) on the net entropy generation rate of the system as obtained with a change in $\overline{\text{Pe}}$, is depicted in Fig. 8.

Before we started discussing the variation of global entropy generation in the system as seen in Fig. 7a, b, we would like to recall the physical significance of the Peclet numbers defined in this analysis. Note that the Peclet number signifies the proportion between the convective heat transfer and diffusive heat transfer rates. Accordingly, an increase in the magnitude of $\overline{\text{Pe}}$ signifies either an increment in the convective transport of heat or decrement in the conductive heat transfer through the fluid. With an increasing value of the $\overline{\text{Pe}}$ in the range $0 < \overline{\text{Pe}} < \overline{\text{Pe}}_{\text{opt}}$, the convective heat transport

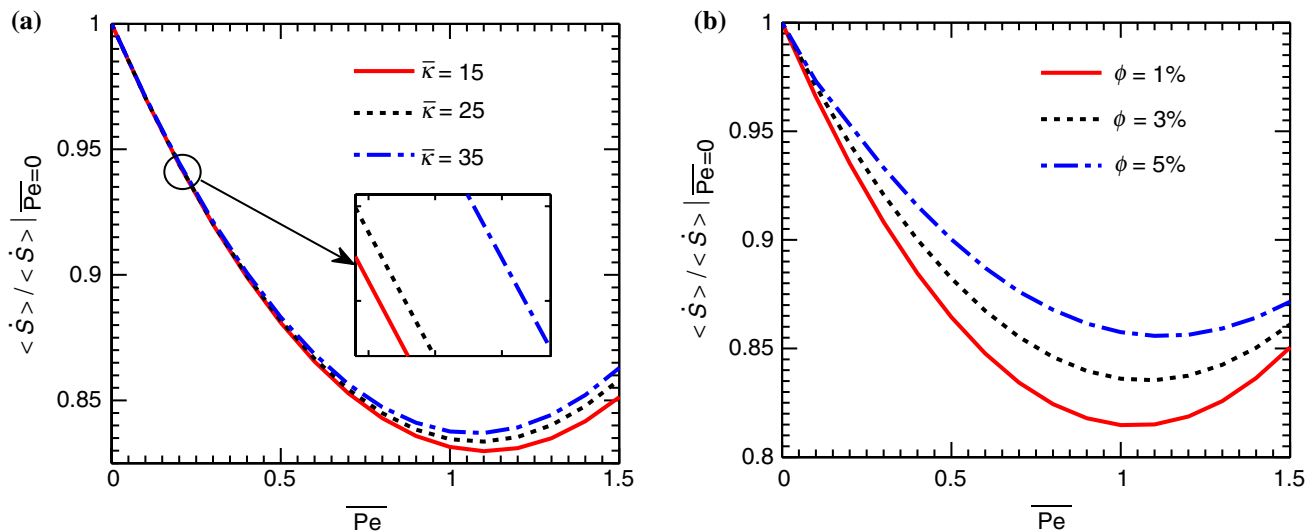


Fig. 7 Disparity of the normalized global entropy generation rate as a function of dimensionless Peclet number of nanofluid ($\overline{\text{Pe}}$); **a** for $\phi = 3\%$ and different value of $\bar{\kappa}$; **b** for $\bar{\kappa} = 20$ and different value of

ϕ . Other parameters are: $p_x = 1$, $\text{Br} = 0.1$, $J = 1$, $\text{Bi}_1 = 2$, $\text{Bi}_2 = 15$, $\gamma_1 = 10$, $\delta_1 = \delta_2 = 0.1$, and $\gamma_2 = 15$. The CPU time for $\bar{\kappa} = (15, 25, 35)$ and $\phi = (1, 3, 5)$ are (154.91, 188.65, 227.5) s and (181.35, 177.74, 167.01) s, respectively

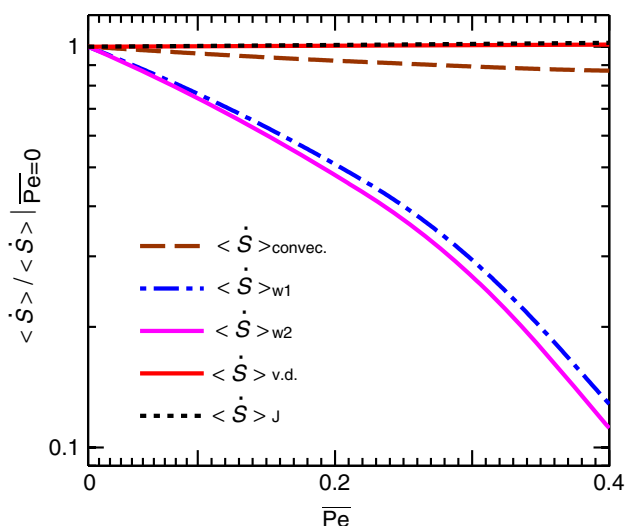


Fig. 8 Disparity of normalized global entropy generation rate of the individual terms associated with Eq. (33) as a function of \overline{Pe} . Other parameters are: $p_x = 1$, $Br = 0.1$, $J = 1$, $Bi_1 = 2$, $Bi_2 = 15$, $\gamma_1 = 10$, $\delta_1 = \delta_2 = 0.1$, and $\gamma_2 = 15$

through the fluid will increase, and fluid temperature will decrease. Because of this decrease in the fluid temperature, heat conduction through the walls of the channel will decrease, and the overall effect will result in a reduction in system entropy generation as confirmed by the decreasing trend of $\left(\frac{\langle \dot{S} \rangle}{\langle \dot{S} \rangle}|_{\overline{Pe}=0}\right)$ in Fig. 7a, b for $0 < \overline{Pe} < \overline{Pe}_{opt}$. Also, a reduction in $\langle \dot{S} \rangle_{w1}$ and $\langle \dot{S} \rangle_{w2}$ in this regime of $0 < \overline{Pe} < \overline{Pe}_{opt}$ is confirmed in Fig. 8. However, as the Peclet number increases beyond its optimum value ($\overline{Pe} > \overline{Pe}_{opt}$), a significant enhancement in convective transport of heat through the fluid governs the system entropy generation as realized by a further increasing trend in this regime of \overline{Pe} ($\overline{Pe} > \overline{Pe}_{opt}$). From the above discussion, it can be conjectured that the conduction through the walls takes a dominating role in dictating the system entropy generation for $0 < \overline{Pe} < \overline{Pe}_{opt}$, while nanoparticle driven enhancement in convective transport of heat as supported by the viscous dissipation and Joule heating effects becomes the leading character in dictating the system entropy generation for $\overline{Pe} > \overline{Pe}_{opt}$. As such, our argument is confirmed by the contribution of each term on the net entropy generation in the system as portrayed in Fig. 8 with increasing \overline{Pe} .

Figure 7b describes the effect of nanoparticle volume fraction (ϕ) on the entropy generation rate of the system. It can be observed from Fig. 7b that with increasing ϕ , entropy generation in the system increases for all the value of \overline{Pe} . As mentioned, with an increase in ϕ , both the effective thermal conductivity and effective viscosity of nanofluid increases. Enhancement of convective heat transfer with increasing effective thermal conductivity of the nanofluid strongly

affects the total irreversibility of the system. As a consequence, with increasing ϕ the global entropy generation rate increases, as seen in Fig. 7b. Also, with increasing ϕ , the optimum $\overline{Pe}(\overline{Pe}_{opt})$ for which system entropy generation becomes the minimum becomes slightly higher.

Effect of Biot number (lower wall) on the system irreversibility

In Fig. 9a, b, we show the variation of normalized global entropy generation $\langle \dot{S} \rangle / \langle \dot{S} \rangle|_{Bi_1=0}$ (normalized with its value when $Bi_1 = 0$) versus lower wall Biot number (Bi_1). The other parameters used in plotting the figures have been mentioned in the caption. While Fig. 9a shows the variation for different values of the Debye–Hückel parameter ($\bar{\kappa}$), the effect of nanoparticle volume fraction (ϕ) on the entropy generation rate is demonstrated in Fig. 9b. It may be mentioned here that to explain the variation depicted in Fig. 9a, b, we have depicted the contribution of each term on the system entropy generation rate in Fig. 10. Note that the Biot number is defined as the ratio of the convective heat transfer to the conductive heat transfer in a body. An increase in the magnitude of the Biot number indicates a reduction in the resistance to the surface heat transfer as the properties of the channel wall is remaining fixed. Along these lines, it may be mentioned here that increasing Bi_1 in the range $Bi_1 > Bi_{1,opt}$ stimulates the heat transfer enhancement through the lower wall, leading to an enhancement in system entropy generation rate as seen in Fig. 9a, b. Notably, this phenomenon in the process reduces the fluid temperature and its gradient inside the system. Thus, with the increase in Bi_1 , the entropy generation rate related with the heat transfer through the lower wall ($\langle \dot{S} \rangle_{w1}$) increases, while entropy generation because of the convective heat transfer ($\langle \dot{S} \rangle_{convec.}$) through the fluid gets reduced. These two observations are clearly reflected in Fig. 10, where it is seen that with increasing Bi_1 , $\langle \dot{S} \rangle_{convec.}$ decreases continuously and $\langle \dot{S} \rangle_{w1}$ shows an increasing trend. Also, with a change in Bi_1 in the range $0 < Bi_1 \leq Bi_{1,opt}$, a reduction in fluid temperature and its gradient leads to a decrement in heat transfer between the fluid and upper wall, and overall effect results in a slight reduction in the system entropy generation rate. This complex change of system irreversibility modulated by several factors, as mentioned in Eq. (33) brings about a decreasing-increasing trend of the system entropy generation with a change in Bi_1 as seen in Fig. 9a, b. From the above discussion, it can be concluded that for $0 < Bi_1 \leq Bi_{1,opt}$, heat transfer through the fluid and upper wall takes a lead role in predicting the system entropy generation rate, while for $Bi_1 > Bi_{1,opt}$ conductive heat transfer through lower wall becomes the indicative character for the net thermodynamic irreversibility of the system.

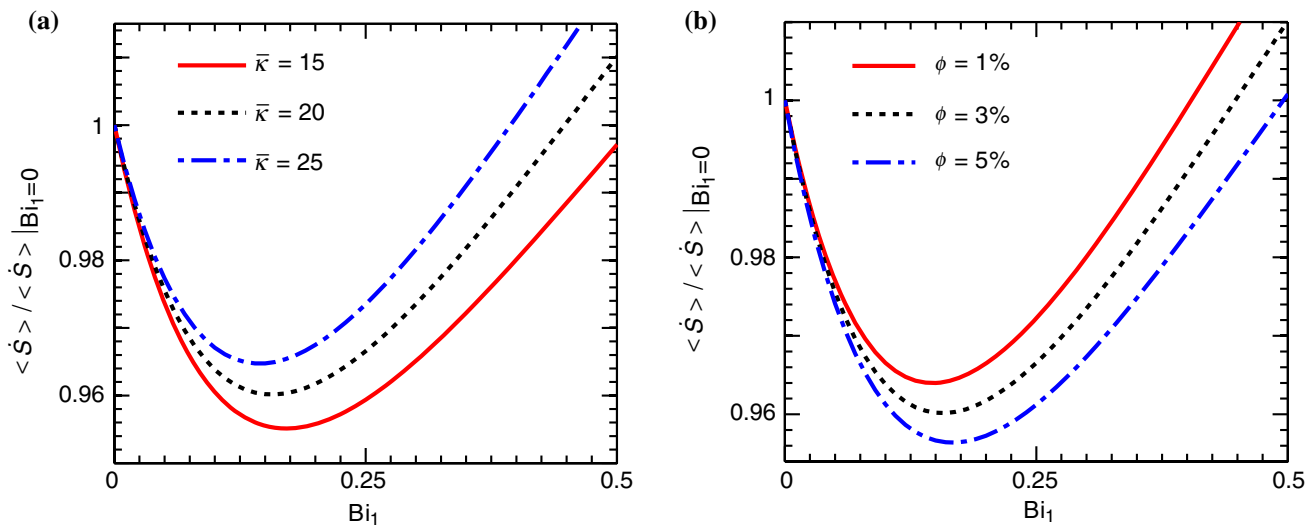


Fig. 9 Disparity of the normalized global entropy generation rate as a function of dimensionless Biot number for the lower wall (Bi_1); **a** for $\phi = 3\%$ and different value of $\bar{\kappa}$; **b** for $\bar{\kappa} = 20$ and different value of ϕ . Other parameters: $p_x = 1$, $Br = 0.1$, $J = 1$, $\delta_1 = \delta_2 = 0.1$,

$Bi_2 = 1$, $Pe = 0.1$, and $\gamma_1 = \gamma_2 = 1$. The CPU time for $\bar{\kappa} = (15, 20, 25)$ and $\phi = (1, 3, 5)$ are (137.86, 140.54, 144.72) s and (143.24, 139.46, 135.54) s, respectively

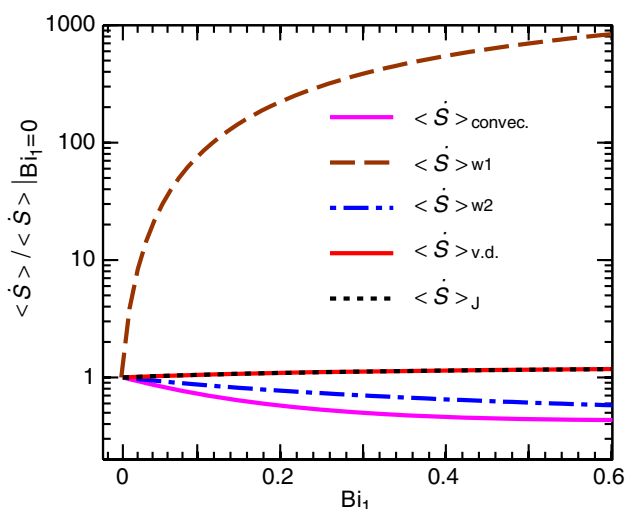


Fig. 10 Disparity of normalized global entropy generation rate of the individual terms associated with Eq. (33) as a function of Bi_1 ; Other parameters: $p_x = 1$, $Br = 0.1$, $J = 1$, $\delta_1 = \delta_2 = 0.1$, $Bi_2 = 1$, $Pe = 0.1$, and $\gamma_1 = \gamma_2 = 1$

A relative increment in system entropy generation with increasing value of $\bar{\kappa}$ as seen in Fig. 9a is attributed effect of viscous dissipation dominated irreversibility of system, largely stemming from electrical force modulated enhancement in the flow velocity and its gradient inside the EDL (see Fig. 2b for flow velocity with $\bar{\kappa}$). Figure 9b shows the impact of the volume fraction of nanoparticle in carrier fluid (ϕ) on the entropy generation rate. The volume fraction of nanoparticle affects the convective heat transfer by

modulating the thermal conductivity. Also, an increment in ϕ will stimulate the viscous dissipation effect following the enhancement in the effective viscosity of the fluid. For this case, as clearly seen from Fig. 10, irreversibility due to viscous heating that too becomes severe with increasing ϕ surpasses the irreversibility that is stemming from the convective transport of heat (which becomes stronger with increasing ϕ as well). Thus, a rise in fluid temperature with increasing ϕ (due to higher viscous dissipation) will lead to a reduction in the conductive transport of heat through the lower wall, which is the influencing factor in dictating the system irreversibility. Because of this phenomenon, with the increasing ϕ , the entropy generation rate in the system reduces (relatively), as seen in Fig. 9b with a slight shift in $Bi_{1,opt}$ towards its higher value.

Conclusions

We have investigated the entropy generation characteristics for a conjugate heat transfer problem, wherein, a nanofluid, driven under the combined influence of an externally imposed pressure gradient and electroosmosis, is subjected to an asymmetric cooling at the channel walls. For this thermo-fluidic transport process, taking accounts of the viscous dissipation and Joule heating effects, we have established that the net entropy generation rate of the system is an outcome of the intricate interplay between the irreversibilities associated with heat transfer, viscous dissipation, and Joule heating. It is found that such an interplay among these irreversibilities gives rise to an optimum value of the

geometrical parameter, viz. the channel wall thickness (δ), and the thermophysical parameters viz., the thermal conductivity of the wall (γ), Biot number (Bi), and the modified Peclet number (Pe), leading to the minimum entropy generation rate of the system. This study further reveals that changes in the electroosmotic parameter $\bar{\kappa}$ (representative of the EDL thickness) or the composition of the fluid (ϕ , the volume fraction of nanoparticles agglomerates) can non trivially alter the optimum values of these parameters. We believe such an analysis will be helpful in optimum design of the thermal systems/devices typically used in microscale thermal management such as micro-heat exchangers, micro-reactors, and micro heat pipes.

Acknowledgements PKM wishes to acknowledge the financial support received from DST-SERB through Grant No. ECR/2016/000702/ES.

References

- Gould C, Shammam N. A review of thermoelectric MEMS devices for micro-power generation, heating and cooling applications. In: *Micro Electron Mech Syst. InTech*; 2009.
- Avci M, Aydın O, Emin Arıcı M. Conjugate heat transfer with viscous dissipation in a microtube. *Int J Heat Mass Transf.* 2012;55:5302–8.
- Horiuchi K, Dutta P, Hossain A. Joule-heating effects in mixed electroosmotic and pressure-driven microflows under constant wall heat flux. *J Eng Math.* 2006;54:159–80.
- Sánchez S, Arcos J, Bautista O, Méndez F. Joule heating effect on a purely electroosmotic flow of non-Newtonian fluids in a slit microchannel. *J Nonnewton Fluid Mech.* 2013;192:1–9.
- Raja M, Vijayan R, Dineshkumar P, Venkatesan M. Review on nanofluids characterization, heat transfer characteristics and applications. *Renew Sustain Energy Rev.* 2016;64:163–73.
- Kleinstreuer C, Feng Y. Experimental and theoretical studies of nanofluid thermal conductivity enhancement: a review. *Nanoscale Res Lett.* 2011;6:229.
- Mahian O, Kianifar A, Kleinstreuer C, Al-Nimr MA, Pop I, Sahin AZ, et al. A review of entropy generation in nanofluid flow. *Int J Heat Mass Transf.* 2013;65:514–32.
- Prasher R, Bhattacharya P, Phelan PE. Thermal conductivity of nanoscale colloidal solutions (nanofluids). *Phys Rev Lett.* 2005;94:025901.
- Xuan Y, Li Q, Zhang X, Fujii M. Stochastic thermal transport of nanoparticle suspensions. *J Appl Phys.* 2006;100:043507.
- Das K. Nanofluid flow over a shrinking sheet with surface slip. *Microfluid Nanofluidics.* 2013;16:391–401.
- Brinkman HC. The viscosity of concentrated suspensions and solutions. *J Chem Phys.* 1952;20:571.
- Kumar Mondal P, Wongwises S. Magneto-hydrodynamic (MHD) micropump of nanofluids in a rotating microchannel under electrical double-layer effect. *Proc Inst Mech Eng Part E J Process Mech Eng.* 2020;234:318–30.
- Wang X, Xu X, Choi SUS. Thermal conductivity of nanoparticle—fluid mixture. *J Thermophys Heat Transf.* 1999;13:474–80.
- Huminc G, Huminc A. Heat transfer capability of the hybrid nanofluids for heat transfer applications. *J Mol Liq.* 2018;272:857–70.
- Choi SUS. Enhancing thermal conductivity of fluids with nanoparticles. *Am Soc Mech Eng Fluids Eng Div FED.* 1995;231:99–105.
- Sheikholeslami M, Ashorynejad HR, Rana P. Lattice Boltzmann simulation of nanofluid heat transfer enhancement and entropy generation. *J Mol Liq.* 2016;214:86–95.
- Bejan Adrian. *Entropy generation minimization: the method of thermodynamic optimization of finite-size systems and finite-time processes.* 1st ed. Boca Raton: CRC Press; 1995.
- Bejan A, Kestin J. Entropy generation through heat and fluid flow. *J Appl Mech.* 1983;50:475.
- Bejan A. Entropy generation minimization: the new thermodynamics of finite-size devices and finite-time processes. *J Appl Phys.* 1996;79:1191–218.
- Sarma R, Jain M, Mondal PK. Towards the minimization of thermodynamic irreversibility in an electrically actuated microflow of a viscoelastic fluid under electrical double layer phenomenon. *Phys Fluids.* 2017;29:103102.
- Sarma R, Mondal PK. Entropy generation minimization in a pressure-driven microflow of viscoelastic fluid with slippage at the wall: effect of conjugate heat transfer. *J Heat Transf.* 2018;140:052402.
- Mah WH, Hung YM, Guo N. Entropy generation of viscous dissipative nanofluid flow in microchannels. *Int J Heat Mass Transf.* 2012;55:4169–82.
- Ting TW, Hung YM, Guo N. Entropy generation of viscous dissipative nanofluid flow in thermal non-equilibrium porous media embedded in microchannels. *Int J Heat Mass Transf.* 2015;81:862–77.
- Kaushik P, Mondal PK, Chakraborty S. Flow dynamics of a viscoelastic fluid squeezed and extruded between two parallel plates. *J Nonnewton Fluid Mech.* 2016;227:56–64.
- Kaushik P, Mondal PK, Pati S, Chakraborty S. Heat transfer and entropy generation characteristics of a non-Newtonian fluid squeezed and extruded between two parallel plates. *J Heat Transf.* 2017;139:022004.
- Mondal PK, Mukherjee S. Viscous dissipation effects on the limiting value of Nusselt numbers for a shear driven flow between two asymmetrically heated parallel plates. *Front Heat Mass Transf.* 2012;3:033004.
- Jacobson SC, McKnight TE, Ramsey JM. Microfluidic devices for electrokinetically driven parallel and serial mixing. *Anal Chem.* 1999;71:4455–9.
- Ramos A, editor. *Electrokinetics and electrohydrodynamics in microsystems.* Vienna: Springer Vienna; 2011.
- Tang GY, Yang C, Chai JC, Gong HQ. Joule heating effect on electroosmotic flow and mass species transport in a microcapillary. *Int J Heat Mass Transf.* 2004;47:215–27.
- Horiuchi K, Dutta P. Joule heating effects in electroosmotically driven microchannel flows. *Int J Heat Mass Transf.* 2004;47:3085–95.
- Gaikwad HS, Roy A, Mondal PK, Chimres N, Wongwises S. Irreversibility analysis in a slip aided electroosmotic flow through an asymmetrically heated microchannel: the effects of joule heating and the conjugate heat transfer. *Anal Chim Acta.* 2019;1045:85–97.
- Oztop HF, Abu-Nada E. Numerical study of natural convection in partially heated rectangular enclosures filled with nanofluids. *Int J Heat Fluid Flow.* 2008;29:1326–36.
- Noreen S, Ain QU. Entropy generation analysis on electroosmotic flow in non-Darcy porous medium via peristaltic pumping. *J Therm Anal Calorim.* 2019;137:1991–2006.
- Nakhchi ME, Esfahani JA. Entropy generation of turbulent Cu-water nanofluid flow in a heat exchanger tube fitted with perforated conical rings. *J Therm Anal Calorim.* 2019;138:1423–36.
- Hajatzadeh Pordanjani A, Aghakhani S, Karimipour A, Afrand M, Goodarzi M. Investigation of free convection heat transfer and entropy generation of nanofluid flow inside a cavity affected

- by magnetic field and thermal radiation. *J Therm Anal Calorim.* 2019;137:997–1019.
36. Sekrani G, Poncet S, Proulx P. Conjugated heat transfer and entropy generation of Al_2O_3 –water nanofluid flows over a heated wall-mounted obstacle. *J Therm Anal Calorim.* 2019;135:963–79.
 37. Darbari B, Rashidi S, Keshmiri A. Nanofluid heat transfer and entropy generation inside a triangular duct equipped with delta winglet vortex generators. *J Therm Anal Calorim.* 2020;140:1045–55.
 38. Goswami P, Mondal PK, Datta A, Chakraborty S. Entropy generation minimization in an electroosmotic flow of non-Newtonian fluid: effect of conjugate heat transfer. *J Heat Transf.* 2016;138:051704.
 39. Sarma R, Gaikwad H, Mondal PK. Effect of conjugate heat transfer on entropy generation in slip-driven microflow of power law fluids. *Nanoscale Microscale Thermophys Eng.* 2017;21:26–44.
 40. Ibáñez G, López A, Cuevas S. Optimum wall thickness ratio based on the minimization of entropy generation in a viscous flow between parallel plates. *Int Commun Heat Mass Transf.* 2012;39:587–92.
 41. Ibáñez G, Cuevas S, López de Haro M. Minimization of entropy generation by asymmetric convective cooling. *Int J Heat Mass Transf.* 2003;46:1321–8.
 42. Gaikwad HS, Basu DN, Mondal PK. Non-linear drag induced irreversibility minimization in a viscous dissipative flow through a micro-porous channel. *Energy.* 2017;119:588–600.
 43. Mohebbi R, Rashidi MM. Numerical simulation of natural convection heat transfer of a nanofluid in an L-shaped enclosure with a heating obstacle. *J Taiwan Inst Chem Eng.* 2017;72:70–84.
 44. Rashad AM, Rashidi MM, Lorenzini G, Ahmed SE, Aly AM. Magnetic field and internal heat generation effects on the free convection in a rectangular cavity filled with a porous medium saturated with Cu–water nanofluid. *Int J Heat Mass Transf.* 2017;104:878–89.
 45. Masliyah JH, Bhattacharjee S. *Electrokinetic and colloid transport phenomena.* Hoboken: Wiley; 2006.
 46. Kunti G, Mondal PK, Bhattacharya A, Chakraborty S. Electrothermally modulated contact line dynamics of a binary fluid in a patterned fluidic environment. *Phys Fluids.* 2018;30:092005.
 47. Sarma R, Deka N, Sarma K, Mondal PK. Electroosmotic flow of Phan-Thien–Tanner fluids at high zeta potentials: an exact analytical solution. *Phys Fluids.* 2018;30:062001.
 48. Sipe JE, Boyd RW. Nonlinear susceptibility of composite optical materials in the Maxwell Garnett model. *Phys Rev A.* 1992;46:1614–29.
 49. Escandón J, Bautista O, Méndez F. Entropy generation in purely electroosmotic flows of non-Newtonian fluids in a microchannel. *Energy.* 2013;55:486–96.
 50. Tang GY, Yang C, Chai CK, Gong HQ. Numerical analysis of the thermal effect on electroosmotic flow and electrokinetic mass transport in microchannels. *Anal Chim Acta.* 2004;507:27–37.
 51. Mondal PK, DasGupta D, Bandopadhyay A, Ghosh U, Chakraborty S. Contact line dynamics of electroosmotic flows of incompressible binary fluid system with density and viscosity contrasts. *Phys Fluids.* 2015;27:032109.
 52. Mondal PK, DasGupta D, Bandopadhyay A, Chakraborty S. Pulsating flow driven alteration in moving contact-line dynamics on surfaces with patterned wettability gradients. *J Appl Phys.* 2014;116:084302.
 53. Mondal PK, DasGupta D, Chakraborty S. Rheology-modulated contact line dynamics of an immiscible binary system under electrical double layer phenomena. *Soft Matter.* 2015;11:6692–702.
 54. Kaushik P, Abhimanyu P, Mondal PK, Chakraborty S. Confinement effects on the rotational microflows of a viscoelastic fluid under electrical double layer phenomenon. *J Nonnewton Fluid Mech.* 2017;244:123–37.
 55. Kaushik P, Mondal PK, Chakraborty S. Rotational electrohydrodynamics of a non-Newtonian fluid under electrical double-layer phenomenon: the role of lateral confinement. *Microfluid Nano-fluidics.* 2017;21:122.
 56. Gaikwad HS, Basu DN, Mondal PK. Slip driven micro-pumping of binary system with a layer of non-conducting fluid under electrical double layer phenomenon. *Colloids Surf A Physicochem Eng Asp.* 2017;518:166–72.
 57. Gaikwad HS, Baghel P, Sarma R, Mondal PK. Transport of neutral solutes in a viscoelastic solvent through a porous microchannel. *Phys Fluids.* 2019;31:022006.
 58. Ghosal S. Electrokinetic flow and dispersion in capillary electrophoresis. *Annu Rev Fluid Mech.* 2006;38:309–38.
 59. Snyder WT. The influence of wall conductance on magnetohydrodynamic channel-flow heat transfer. *J Heat Transf.* 1964;86:552.
 60. Gaikwad HS, Mondal PK, Wongwises S. Non-linear drag induced entropy generation analysis in a microporous channel: the effect of conjugate heat transfer. *Int J Heat Mass Transf.* 2017;108:2217–28.
 61. Mondal PK, Wongwises S. Irreversibility analysis in a low Peclet-number electroosmotic transport through an asymmetrically heated microchannel. *Int J Exergy.* 2017;22:29.
 62. Mondal PK. Thermodynamically consistent limiting forced convection heat transfer in a asymmetrically heated porous channel: an analytical study. *Transp Porous Media.* 2013;100:17–37.
 63. Mondal PK, Wongwises S. Assessment of thermodynamic irreversibility in a micro-scale viscous dissipative circular couette flow. *Entropy.* 2018;20:50.
 64. Mondal PK, Mukherjee S. Viscous dissipation effects on the limiting value of Nusselt numbers for a shear-driven flow through an asymmetrically heated annulus. *Proc Inst Mech Eng Part C J Mech Eng Sci.* 2012;226:2941–9.
 65. Hsieh S-S, Yang T-K. Electroosmotic flow in rectangular microchannels with Joule heating effects. *J Micromech Microeng.* 2008;18:025025.

Publisher's Note Springer Nature remains neutral with regard to jurisdictional claims in published maps and institutional affiliations.